RAA 2018 Vol. **18** No. **3**, 34(6pp) doi: 10.1088/1674–4527/18/3/34

http://www.raa-journal.org *http://iopscience.iop.org/raa*

Research in Astronomy and Astrophysics

Flares before and after coronal mass ejections

Gadikere Sheshagiriyappa Suryanarayana

Indian Institute of Astrophysics, Koramangala, Bengaluru-560034, India; *suryanarayana@iiap.res.in*

Received 2017 July 14; accepted 2017 December 29

Abstract Flare characteristics such as the flare occurrence number density and the distribution of peak flux as well as duration of flares occurring on either side of a coronal mass ejection (CME) onset time are studied. While the flares are rather evenly distributed statistically on either side of the CME onset time, the flare peak flux and duration tend to decrease depending upon their occurrence either before or after the CME onset. This is consistent with the earlier findings that flares emit higher energy before a CME whereas the energy is less in flares occurring after a CME.

Key words: Sun: flares — Sun: flare durations — Sun: peak flux of flares — Sun: coronal mass ejections

1 INTRODUCTION

Flares and coronal mass ejections (CMEs) are known to be independently associated with other phenomena such as shock waves (Cliver et al. 1999). However, their nearly simultaneous occurrence (Munro et al. 1979) has generated much interest in looking at them as either driving the other. But, Harrison (1995) concludes that flares and CMEs are a consequence of the same 'disease' called the magnetic field and changes in it.

Flares have been reported before a CME (Hudson et al. 1996) and after it (Nitta & Akiyama 1999). Aggarwal et al. (2008) reported the occurrence of flares before and after the onset of CMEs. Green et al. (2001) mentioned that flares occur before, during and after a CME launch. They also indicated that flares occurring before a CME launch release more energy than those occurring after it, and the rationale apparently is that the magnetic field contains stored energy and the eruption of a CME removes energy. In this context, we note that the free magnetic energy and *Geostationary Operational Environment Satellite* (*GOES*) flux correlate well (Aschwanden 2013) and the decrease of free energy is associated with the flare (Aschwanden 2015).

Green et al. (2001) have analyzed a few events of CMEs and flares and concluded that occurrence of CME results in flares emitting less energy while also pointing out that flares occurring before CME occurrence tend to be longer in duration and higher in flux emission. Hence, a statistical study on the number density of flare occurrences before and after the CME occurrence and also a comparison of flare peak flux values and durations as a representation of magnitude of flare energy before and after the CME onset is likely to yield interesting insights into the energy dissipation characteristics affected by the CME occurrence. Since the present work is statistical in nature, we do not consider the evolution of sequential flares or flares and CMEs of any specific active region (AR). Also, the nature of duration and peak flux emission of flares without CMEs is not considered. The remaining part of this paper is organized as Data Sets in Section 2, Analysis and Results in Section 3 and Discussion and Conclusion in Section 4.

2 DATA SETS

We seek to meet the objective set out in the Introduction using the durations and peak flux values of soft X-ray flares observed by *GOES* in the 0.05 – 0.4 nm and 0.1 – 0.8 nm wavelength bands (Veronig et al. 2002; Kay et al. 2003) and archived in the Solar Geophysical Data (SGD)[1]. Flares are divided into A, B, C, M and X class as per their peak flux as shown in Table 1.

The association of flares with CMEs, especially the temporal association, poses great uncertainty (Suryanarayana & Balakrishna 2017 and references therein). The Wind WAVES website[2] lists flare-CME association with much better accuracy. Hence, we use the flare-CME associations from this list to compile

[1] *ftp://ftp.ngdc. noaa.gov/STP/SOLAR_DATA/SGD_PDFversion/*
[2] *http://cdaw.gsfc.nasa.gov/CME_list/radio/waves_type2.html*

Table 1 The *GOES* Class of Solar Flare and the Peak Flux Range

GOES Class	W m^{-2}	erg cm^{-2} s^{-1}
A	$\phi < 10^{-7}$	$\phi < 10^{-4}$
B	$10^{-7} \leq \phi < 10^{-6}$	$10^{-4} \leq \phi < 10^{-3}$
C	$10^{-6} \leq \phi < 10^{-5}$	$10^{-3} \leq \phi < 10^{-2}$
M	$10^{-5} \leq \phi < 10^{-4}$	$10^{-2} \leq \phi < 10^{-1}$
X	$10^{-4} \leq \phi$	$10^{-1} \leq \phi$

a list of flares with associated CMEs. We have tabulated a list of 143 flares occurring within $\pm$1 hour from the onset of CMEs for the period Mar. 1997 to Oct. 2002. We collect the CME onset times from the *Solar and Heliospheric Observatory* (*SOHO*) Large Angle Spectroscopic Coronagraph (LASCO) archive [3]. CMEs are first observed when they are in the LASCO C2 field of view which is $\sim$ 1.5 solar radii from the center of the Sun. Hence, a reasonable comparison with flare start times cannot be made with the first appearance in the LASCO C2 field of view. Since our aim is to compare the peak flux and duration of flares on the basis of their occurrence time with respect to the CME occurrence, we collect the CME onset times from the individual text file reported for each CME as given in the CME catalog instead of the first appearance time of the CME in the LASCO C2 field of view.

3 ANALYSIS AND RESULTS

Using the height and time values provided in the CDAW text files, the CME onset times are estimated by fitting the linear and quadratic fits to height time plots. These plots are the same as provided in the *SOHO* LASCO catalog. Figure 1(a) and (b) displays examples of linear and quadratic fits for a sample of data. In the inset equation, H and T represents the height and time of the CME respectively. We estimate the uncertainty in the onset time so obtained by considering the example of the CME reported on 2000 January 02, 13:54:06 UT. That CME has been reported with eight height time values. We estimate the onset time uncertainty by adopting the formulas presented in Bevington & Robinson (2003) where equation (6.15) and equation (7.11) provide the methodology for estimating the uncertainty in the linear fit and quadratic fit, respectively. Adopting these formulas, we get $\sigma = \sqrt{\sum (H_i - a_1 - a_2 T_i)^2/(N-m)}$ and $\sigma = \sqrt{\sum (H_i - (a_1 + a_2 T_i + a_3 T_i^2))^2/(N-m)}$, where σ is the uncertainty, H and T are the height and time respectively, a_1, a_2 and a_3 are fitted parameters, N is the number of data points and m is the number of free parameters or number of fitted parameters. The linear fit and quadratic fit onset time uncertainties thus obtained for the example mentioned above are 0.1619 and 0.1932, respectively. The complete range of uncertainties in onset values for all the CMEs varies between 0.0079 & 0.4153 and 0.0133 & 0.2851 for linear and quadratic fits, respectively. Since these values are too small compared to onset times, they are not visible in Figure 2(a).

We use both onset1 and onset2. The CME onset1 and onset2 times are obtained by extrapolating the linear fit and the quadratic fit to the solar surface, respectively (Gopalswamy et al. 2009). In order to ascertain whether the onset1 and onset2 times vary widely, we plot the two sets of values in Figure 2(a). A correlation coefficient of 99.87% with a significance of $\sim 100\%$ confirms that the onset times obtained using the linear fit and the quadratic fit yield almost the same onset times. We also compute the difference between the onset1 time and onset2 time of each CME and plot the number of CMEs in each time difference as a histogram in Figure 2(b), which shows that over 92% of CMEs have an onset1 and onset2 time difference of less than 24 min from each other. This reinforces the view that the onset times obtained using linear and quadratic fits do not diverge significantly.

The source ARs of CMEs are distributed from the solar disk center to the limb. It can be expected to introduce a maximum error of 1 solar radius into determination of the height when the CME originates. This is the case if all CMEs originate close to the disk center. As the event occurrence can be expected to be distributed evenly from the disk center to the limb, the computation of onset time error reduces from the disk center to the limb. Shen et al. (2013) reported that in the case of full halo CMEs, the CMEs away from the disk center suffer much less from the projection effect, especially if their speeds are more than 900 km s^{-1}. Furthermore, Zhao et al. note that only 118 CMEs display a non-radial propagation out of 841 CMEs observed between 1996 and 1998. Considering the fact that source locations of the CMEs from the geometrical methods are consistent with the flaring locations, Lee et al. (2014) suggested that most CMEs are radially ejected. They estimated different parameters of CMEs using different geometrical models and also by direct measurement, and found that velocity estimates closely match between different models as well as direct measurement. Hence, we assume that the onset times obtained by linear and quadratic fits to height time measurements yield onset times that fairly match those obtained by different models.

The CMEs are accelerated exponentially, especially in the lower atmosphere. A linear or quadratic extrap-

[3] *http://cdaw.gsfc.nasa.gov/CME_list/*

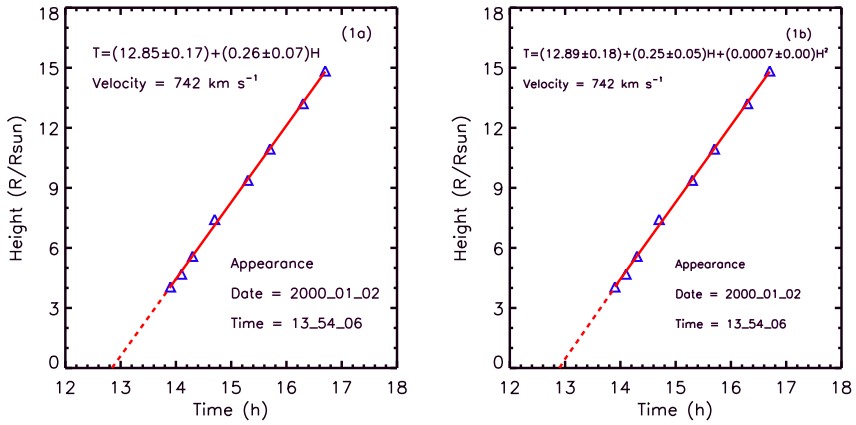

Fig. 1 Fig. 1(a) shows the linear fit and Fig. 1(b) shows the quadratic fit with which the extrapolated start times (shown as *dashed extrapolations*) are determined for the CMEs from the height-time plots. T and H indicate the time and height, respectively.

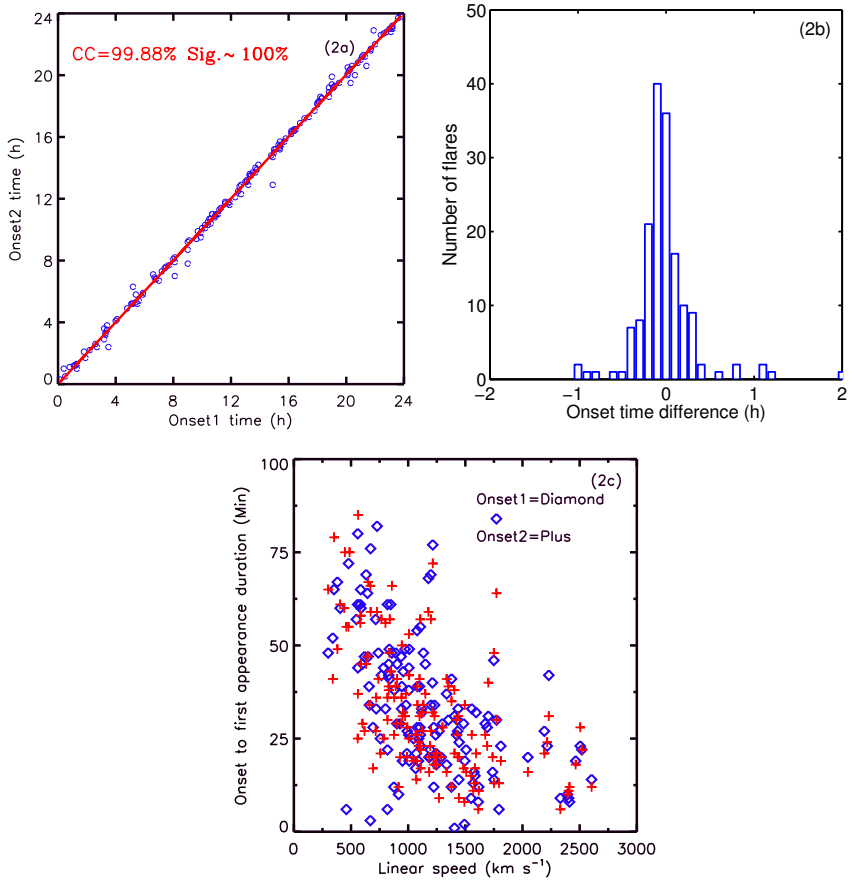

Fig. 2 Figure 2(a) shows the correlation of onset1 and onset2 times for CMEs. The *solid line* represents the linear least-squares fit. The onset times are as given in the text file for each CME in the database. Fig. 2(b) displays the number of CMEs in each value of the difference between the onset1 time and onset2 time. More than 92% of CMEs lie between the time difference of ± 24 min of each other. Fig. 2(c) plots the duration between estimated onset time and first appearance time against the linear speed of the CME.

olation from height-time profiles of CMEs originating close to the disk center cannot predict the correct time for CME onset. This may introduce a high uncertainty in the estimation of onset time, especially if they are originating near the disk center. Hence, we compute the duration between the estimated onset time and the first appearance time in the LASCO C2 field of view. We plot the linear speed and this duration in Figure 2(c).

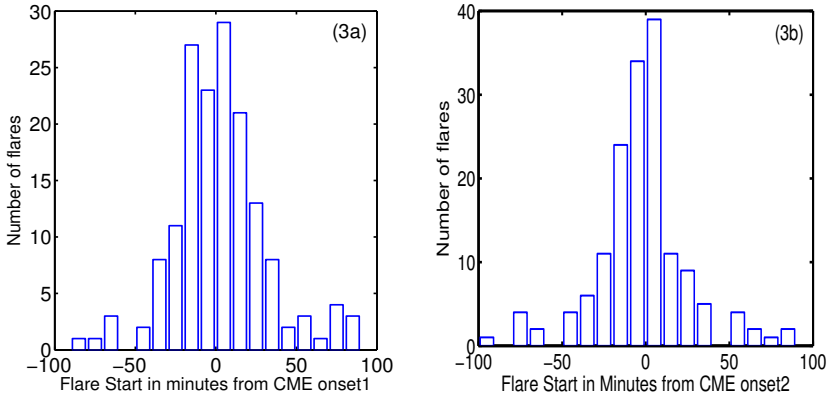

Fig. 3 A bar graph that shows that an even number of flares occur before and after the CME onset1 (a) and onset2 (b) times.

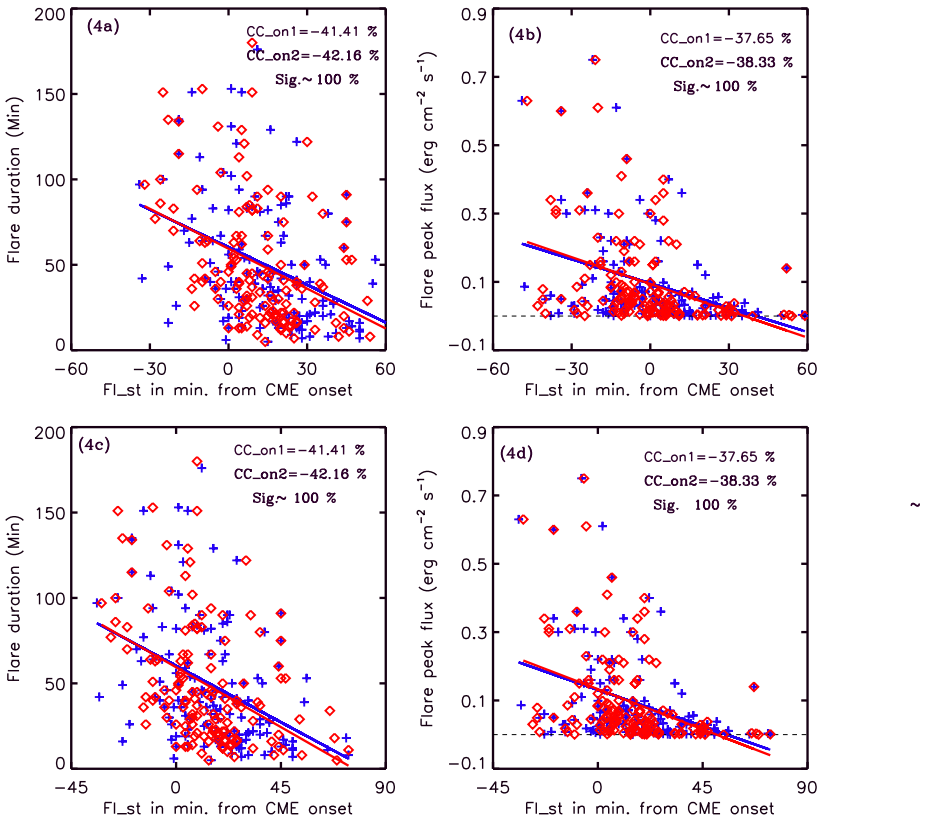

Fig. 4 Graphs illustrating the durations of flares (a) and peak flux of flares (b) occurring before and after the CME onset time. *Plus* symbols in *blue* and *diamonds* in *red* represent the flares occurring with respect to CME onset1 and onset2 times, respectively. The 100% significance indicated is for both the data distributions. CC_on1 represents the correlation coefficient for flare distributions about the onset1 time of the CME and CC_on2 represents the correlation coefficient for flare distributions about the onset2 time of the CME. Fl_st stands for the flare start time with respect to CME onset time. The horizontal dashed line in (b) and (d) marks $y = 0$. (c) and (d) represent the decrease of flare duration and peak flux as a function of their occurrence with respect to the CME onset time artificially advanced by an average of 15 min. The correlation coefficients and significance values are also the same for these plots.

We note that over 80% of CMEs have a duration of less than 50 min. The average value of this duration is 34.10±18.66 min and 32.87±17.32 min, respectively for onset1 and onset2. Furthermore, in the present sample, almost all CMEs with duration less than 50 min have a linear speed of over 500 km s^{-1}. Hence, considering the fact that much of the acceleration is imparted before the CME reaches the LASCO C2 field of view (Bein et al.

2011), the onset times obtained from predominantly high speed CMEs are likely to be nearer to the actual onset time.

Harrison (1995) notes that for CMEs well out of the plane of the sky, actual onset may precede the projected onset as the source region is well onto the disc. He further concludes that since this is a rather small effect, the projected onset time would be 7 to 1.6 min earlier than the limb projected onset for speeds of 100 km s^{-1} to 450 km s^{-1} for CME source regions about 30° out of the plane of the sky. However, in our sample, most of the CMEs exhibit speeds exceeding 500 km s^{-1}.

Moreover, Jain et al. (2010) suggest that the onset time of a flare and CME in their investigation is ±40 min. They indicate that in 62% of cases studied, the onset time of CMEs precedes the onset of flares by tens of minutes. Yashiro & Gopalswamy (2008) conclude that the difference between the flare and the CME onset displays a Gaussian distribution with a standard deviation of 17 and 15 min, respectively, for the first and second order extrapolated onsets. Studying 10 events, Howard & Harrison (2004) reported that surface eruptions observed in the Extreme ultraviolet Imaging Telescope were found around the projected time of CME onset obtained by the extrapolation method for LASCO CMEs.

Coronal dimming is considered as the signature of mass ejection whose region could vary in height between 1.1 to 2.5 solar radii (Howard & Harrison 2004 and references therein). Harrison & Lyons (2000) note that there is no reason to assume that CMEs originate from the surface which means the extrapolated onset time could precede the actual onset time. Therefore, contrasting this with the scenario that estimated onset time would be generally later than the actual onset time (Harrison 1995), the actual onset time would lie somewhere between the onset determined by the coronal dimming method and the extrapolation method. Vasanth et al. (2011) suggest that these two aspects minimize the extrapolated onset time error to within 10 min. Hence, we regard the uncertainty in estimated onset times as not too significant in adversely affecting our results.

In order to determine whether a flare has started before the onset of CME or after, we subtract the CME onset time from the flare start time. Thus the negative and positive values represent flares starting before and after the CME onset, respectively. We bin the number of flares in intervals of 10 min on either side of the CME onset. The histograms in Figure 3(a) and Figure 3(b) represent the distribution of flares on either side of the CME onset1 and onset2, respectively. We find that the flares are quite evenly distributed before and after the occurrence of CMEs, with density of flare occurrence peaking close to CME onset. Thus, in a statistical sense, the flares occur rather evenly on either side of the CME onset.

In order to know the association between the time of flare occurrence from the CME onset time and the flare duration, in Figure 4(a) we plot the durations of flares against flare occurrence time. The negative and positive values along the x axis represent the time of flare occurrence before and after the CME, respectively, corresponding to onset1 and onset2. This figure demonstrates with high significance that the durations of flares tend to decrease as they occur from before the CME onset to later. This phenomenon is repeated in terms of flare peak flux values as seen in Figure 4(b). The continuous lines in blue and red represent the linear least-squares fits for flares occurring with respect to onset1 and onset2 times of CMEs. The CC values inset in the figures represent respective correlation coefficients. The significance of correlations for respective data sets in each plot is also shown. Fl_st is the flare start time in the figures where it occurs. The scatter plots in Figure 4(a) and Figure 4(b) represent unbinned data points. A given CME is provided with two onset times and hence the same flares are used for both onset1 and onset2 times of CMEs.

It is suggested that the extrapolated onset time is later than the true onset (Harrison 1995) and this could even be as high as 30 min in a few cases. While the discussion at the beginning of this section is expected to considerably address this concern, as a further check to mitigate this aberration, in Figure 4(c) we plot the flare duration as a function of their occurrence with respect to the extrapolated onset time of the CME arbitrarily advanced by an average of 15 min. Similarly, we plot the peak flux in Figure 4(d). We find that the same tendency of the flare duration and peak flux decreasing as a function of their occurrence prevails with respect to the artificially advanced CME onset time. Hence, the onset time error apparently does not affect our results.

4 DISCUSSION AND CONCLUSIONS

Using the Wind WAVES list of flare-CME associations, the SGD archive for flare durations and peak flux values and the *SOHO* LASCO archive for CME onset times, we study the behavior of the peak flux and duration of soft X-ray flares by considering the occurrence of flares with respect to the onset time of CMEs for the period Mar. 1997 to Oct. 2002. We found that the peak flux and duration values decrease as the flares occur from before the CME onset to the time after the CME onset. This is consistent with the finding by Green et al. (2001) that flares occurring before the CME have a larger spread in

intensity and duration, while the flares occurring after the CME are shorter and less intense. They suggest that the CME launch leads to a reduction in the energy content of the AR magnetic field.

Liu et al. (2010) suggest that the pre-CME structure is of great importance to understanding the origin of CMEs, demonstrating that the gradual inflation associated with 16 AR coronal arcades leads to CMEs. They report an inflation duration of 8.7 ± 4.1 h. Hence, the time separation between the flare start and CME onset could be reflecting the appropriation of available energy into the emission of the flare and creating a situation with insufficient flux to drive the CME. Thus, if a flare has higher emission, more time is needed to accumulate energy to inflate the arcade and the consequent mass ejection. By this logic, if the emission of the flare is greater, the delay in ensuring the ejection of mass will be greater, and by some unknown process, the energy not utilized by the flare is required to drive the mass ejection. Assuming that is true, this remaining energy is insufficient to trigger the CMEs, and prolonged duration after a flare will play a role in re-energizing the region before ensuring a CME occurrence. A probable demonstration of this suggestion can be gleaned from the observation by Ravindra et al. (2011) that the decrease in total absolute current indicates that the free energy for flare and CME was supplied from the AR and there exists a time delay between the start of the free energy and the emission of this energy through the flare and CME. It is suggested that this indicates the relationship between the time delay from flare to CME and CME to flare and the magnitude of flare energy.

Overall, we note that the results presented in the current study agree with earlier studies that the flares tend to occur with decreasing energy from before the CME to after it. This is consistent with the view that a common process of build up and long term evolution of magnetic field could be behind the flare and CME (Green et al. 2001).

Acknowledgements My sincere thanks go to the referee for suggesting important corrections. We thank the Wind WAVES team for the flare-CME associations. Soft X-ray flare data are from the Solar Geophysical Data archive. This CME catalog is generated and maintained at the CDAW Data Center by NASA and The Catholic University of America in cooperation with the Naval Research Laboratory.

References

Aggarwal, M., Jain, R., Mishra, A. P., et al. 2008, Journal of Astrophysics and Astronomy, 29, 195
Aschwanden, M. J. 2013, Sol. Phys., 287, 369
Aschwanden, M. J. 2015, ApJ, 804, L20
Bein, B. M., Berkebile-Stoiser, S., Veronig, A. M., et al. 2011, ApJ, 738, 191
Bevington, P. R., & Robinson, D. K. 2003, Data Reduction and Error Analysis for the Physical Sciences (3rd edition, MA: McGraw-Hill)
Cliver, E. W., Webb, D. F., & Howard, R. A. 1999, Sol. Phys., 187, 89
Gopalswamy, N., Yashiro, S., Michalek, G., et al. 2009, Earth Moon and Planets, 104, 295
Green, L. M., Harra, L. K., Matthews, S. A., & Culhane, J. L. 2001, Sol. Phys., 200, 189
Harrison, R. A. 1995, A&A, 304, 585
Harrison, R. A., & Lyons, M. 2000, A&A, 358, 1097
Howard, T. A., & Harrison, R. A. 2004, Sol. Phys., 219, 315
Hudson, H. S., Acton, L. W., & Freeland, S. L. 1996, ApJ, 470, 629
Jain, R., Aggarwal, M., & Kulkarni, P. 2010, RAA (Research in Astronomy and Astrophysics), 10, 473
Kay, H. R. M., Harra, L. K., Matthews, S. A., Culhane, J. L., & Green, L. M. 2003, A&A, 400, 779
Lee, H., Moon, Y.-J., Na, H., & Jang, S. 2014, in American Astronomical Society Meeting Abstracts, 224, #224, 218.34
Liu, R., Liu, C., Park, S.-H., & Wang, H. 2010, ApJ, 723, 229
Munro, R. H., Gosling, J. T., Hildner, E., et al. 1979, Sol. Phys., 61, 201
Nitta, N., & Akiyama, S. 1999, ApJ, 525, L57
Ravindra, B., Venkatakrishnan, P., Tiwari, S. K., & Bhattacharyya, R. 2011, ApJ, 740, 19
Shen, C., Wang, Y., Pan, Z., et al. 2013, Journal of Geophysical Research (Space Physics), 118, 6858
Suryanarayana, G. S., & Balakrishna, K. M. 2017, RAA (Research in Astronomy and Astrophysics), 17, 7
Vasanth, V., Umapathy, S., Vršnak, B., & Anna Lakshmi, M. 2011, Sol. Phys., 273, 143
Veronig, A., Temmer, M., Hanslmeier, A., Otruba, W., & Messerotti, M. 2002, A&A, 382, 1070
Yashiro, S., & Gopalswamy, N. 2008, in IAU Symposium, 257, Universal Heliophysical Processes, eds. N. Gopalswamy, & D. F. Webb, 233